Template Synthesis and Photocatalytic Properties of Porous Metal Oxide Spheres Formed by Nanoparticle Infiltration

Dmitry G. Shchukin[†] and Rachel A. Caruso*[,‡]

Max Planck Institute of Colloids and Interfaces, D-14424 Potsdam, Germany, and School of Chemistry, The University of Melbourne, Melbourne, Victoria 3010, Australia

Received February 12, 2004. Revised Manuscript Received March 26, 2004

Porous polymeric beads have been used as templates for the fabrication of porous metal oxide spheres. The beads were soaked in sols of titanium dioxide, zirconium dioxide, iron oxide, aluminum oxide, indium oxide, tin oxide, and cerium oxide. Successful infiltration and templating was obtained for titania, zirconia, tin oxide, and ceria giving monodisperse, nonaggregated spheres with a porous surface and inner structure. The use of iron and aluminum oxide sols resulted in cracked spheres with excess oxide material on the sphere surfaces, and in the case of indium oxide, broken, hollow, shell-like structures were produced. Combining the iron, aluminum, or indium oxide sols with the titania sol, at a 1:1 weight ratio, and impregnating the template produced inorganic spheres containing the two metal oxides. The photocatalytic properties of the titania and mixed titania/indium oxide spheres were studied by monitoring the decomposition of 2-chlorophenol as a function of time and solution pH. Both the porous titania and mixed titania/indium oxide spheres were more efficient photocatalysts than Degussa P25 titania, a commercial standard. Optimum solution pH for the photocatalytic reaction was determined to be pH 6 for the titania spheres and pH 4 for the titania/indium oxide sample. Pyridine adsorption on the mixed titanium/indium oxide spheres showed FTIR peak shifts similar to those of the indium oxide spheres, which indicated the presence of stronger Lewis acid sites compared with the titania spheres.

Introduction

Controlling the morphological properties of materials during synthesis is of great importance, as these structural characteristics strongly influence the performance and purpose of the materials. Templating is an approach which affords the ability to tailor the inner structural arrangements, such as pore size and overall porosity, along with the outer shape and size of the sample.[1] This technique is facile and can be applied with a range of methods for the fabrication of materials including polymers, metal oxides, and metals.

Templates can be used in a number of ways; two methods employ the template as either a medium in which chemical synthesis is performed or as a framework around which preformed particles can be placed. It has been shown that polymer gel and membrane templates can be used in both these ways with either sol−gel reactions being conducted within the porous polymeric structures[2−7] or preformed metal oxide nanoparticles being adsorbed within the pores.[8−11] The final porous monolithic or film structures cannot be dispersed in solution without structural modification to break the samples into smaller pieces. As the ability to disperse the sample is important for various applications, the use of porous polymeric beads as templates to fabricate small (relative to the monolithic, millimeter-size-range, or film, 80-micrometer-thick with varying diameter up to cm, samples) individual components or particles has been pursued. Beads have good packing density and are used extensively in separation applications. However, the fabrication of monodisperse, nonaggregated, porous inorganic spheres remains a challenge.

The templating of "individual entities" requires extreme care to allow infiltration and coating while preventing aggregation of the material. Little work has been conducted using porous spherical templates for the fabrication of inorganic systems. Once control parameters have been found, templating approaches for the formation of porous inorganic spheres are facile and allow manipulation of sphere diameter and pore size,

* To whom correspondence should be addressed. Fax: +61 3 9347 5180. E-mail: RCaruso@unimelb.edu.au.
[†] Max Planck Institute of Colloids and Interfaces.
[‡] The University of Melbourne.

(1) Caruso, R. A. *Top. Curr. Chem.* **2003**, *226*, 91.
(2) Caruso, R. A.; Giersig, M.; Willig, F.; Antonietti, M. *Langmuir* **1998**, *14*, 6333.
(3) Caruso, R. A.; Antonietti, M.; Giersig, M.; Hentze, H.-P.; Jia, J. *Chem. Mater.* **2001**, *13*, 1114.
(4) Schattka, J. H.; Shchukin, D. G.; Jia, J.; Antonietti, M.; Caruso, R. A. *Chem. Mater.* **2002**, *14*, 5103.
(5) Caruso, R. A.; Schattka, J. H. *Adv. Mater.* **2000**, *12*, 1921.
(6) Yang, D.; Qi, L.; Ma J. *Adv. Mater.* **2002**, *14*, 1543.
(7) Yang, D.; Qi, L.; Ma J. *J. Mater. Chem.* **2003**, *13*, 1119.
(8) Breulmann, M.; Davis, S. A.; Mann, S.; Hentze, H.-P.; Antonietti, M. *Adv. Mater.* **2000**, *12*, 502.
(9) Shchukin, D. G.; Schattka, J. H.; Antonietti, M.; Caruso, R. A. *J. Phys. Chem. B* **2003**, *107*, 952.
(10) Shchukin, D. G.; Caruso, R. A. *Adv. Funct. Mater.* **2003**, *13*, 789.
(11) Wang, Y.; Tang, Y.; Dong, A.; Wang, X.; Ren, N.; Shan, W.; Gao, Z. *Adv. Mater.* **2002**, *14*, 994.

10.1021/cm0497780 CCC: $27.50
Published on Web 05/07/2004

as determined by the initial template bead. We have recently shown that porous polymeric beads can be successfully templated using sol−gel chemistry for the fabrication of silica and titania spheres.[12] Porous gold spheres have also been obtained using preformed 4-(dimethylamino)pyridine (DMAP) stabilized gold nanoparticles and polystyrene/divinyl benzene beads.[13] This approach has been extended here to obtain a number of monodisperse porous metal oxide spheres plus mixtures of titania and aluminum oxide, indium oxide, or iron oxide.

Metal oxides with controlled porosity have been fabricated for applications such as fuel cells, photonics, and catalysis. Titanium dioxide, a semiconducting ceramic, has been intensely studied for its photocatalytic properties.[14,15] The inclusion of another metal oxide within the titanium dioxide structure has been shown to positively influence the photocatalytic efficiency of titania.[4,9,16−18] In this article, structural and compositional properties of metal oxide spheres obtained by using porous polymeric beads as templates are studied. The photocatalytic activity of the titania spheres is compared with Degussa P25 titania and the mixed TiO_2/In_2O_3 sample. The advantage of the porous micrometer-sized spherical samples is that they are more easily removed from solution than nanoparticles, while exhibiting significant surface areas.

Experimental Section

Materials. The template beads, polystyrene cross-linked with divinyl benzene, were obtained from Amersham Biosciences (Uppsala, Sweden) (Trade name: Source 15 ETH. These beads are hydroxyl functionalized with an average dry diameter of 11.5 μm). The following precursors were utilized for the synthesis of the nanosized metal oxide particles: $TiCl_4$, $ZrO(NO_3)_2$, $Fe(NO_3)_3 \cdot 9H_2O$, $AlCl_3$, $In(NO_3)_3 \cdot 5H_2O$, $SnCl_4$, and $(NH_4)_2Ce(NO_3)_6$. These precursors, HCl, NaOH, H_2SO_4, HNO_3, and a 25% aqueous solution of ammonia were purchased from Aldrich.

All chemicals were used as received. The water used in all experiments was prepared in a three-stage Millipore Milli-Q Plus 185 purification system and had a resistivity higher than 18 MΩ cm.

Sol Synthesis. A previously published procedure was followed for the synthesis of the metal oxide sols.[19] The inorganic precursor (0.027 mol) was dissolved in 0.5 M aqueous HCl (20 mL). The precursor was hydrolyzed by the addition of a 12.5 wt. % aqueous ammonia solution with vigorous stirring of the solution at 0 °C, until a pH value of 5−6 was reached. The precipitate obtained was washed with water and centrifugation/decantation cycles until a turbid supernatant solution was obtained. To redisperse the particles, all of the oxide sols except SnO_2 were then sonicated (10 min in a Transsonic Digitals bath sonifier) after the addition of concentrated nitric acid (1 mol HNO_3 per 5 mol of resulting oxide) as a stabilizer. For SnO_2, small amounts of aqueous ammonia were used to stabilize the nanoparticles. The sols were then dialyzed against Milli-Q water employing a Spectra/Por membrane (MWCO: 6−8000) to adjust the pH of the solution to between 3 and 5. The properties of the final sols used in the templating procedure are shown in Table 1.

Table 1. Concentration (*C*) of the Synthesized Metal Oxide Sols and Diameter (*d*) and Crystallinity of the Nanoparticles

metal oxide	*C* (wt. %)	*d* (nm)	crystallinity
TiO_2	7.0	4	anatase/rutile
ZrO_2	6.4	10	amorphous
Fe_2O_3	5.6	6	hematite
Al_2O_3	5.0	12	amorphous
In_2O_3	6.8	6	amorphous
SnO_2	6.2	4	amorphous
CeO_2	12.5	4	amorphous

Templating Procedure. To infiltrate the polymer beads with the oxide particles, the dried organic template material (0.1 g) was soaked with stirring in the corresponding metal oxide sols (5 mL), or their mixtures, for 48 h at room temperature. The solution was then centrifuged to obtain the metal oxide/bead composite, excess nanoparticles were removed by washing with water followed by centrifugation, and the sample was dried at 60 °C for 1 h. Calcination at 500 °C (with a heating rate of 8 °C min^{-1}) was conducted for 5 h in an oxygen atmosphere to remove the template.

Characterization. A Zeiss DSM 940 scanning electron microscope (SEM) and a Gemini Leo 1550 SEM were used to examine the structure of the metal oxide materials. To view the inner texture of the metal oxide spheres a Zeiss EM 912 Omega transmission electron microscope (TEM) was employed. Before TEM investigation the samples were set in poly(methyl methacrylate) and then they were sliced into ultrathin sections (30 to 100 nm thick) using a Leica ultracut UCT ultramicrotome. Carbon-coated copper grids were used to support the thin sections.

Thermogravimetric analysis (TGA) of the metal-oxide-loaded polymer beads was performed to determine the inorganic loading in the polymer beads using a Netzsch TG 209 apparatus. A Micromeritics TriStar 3000 surface area and pore analyzer was employed to obtain the specific surface area using BET analysis after N_2 adsorption. Wide-angle X-ray scattering was conducted to investigate the crystal structure of the materials using an Enraf-Nonius PDS-120 apparatus.

To characterize the surface acidity of the oxide samples, the adsorption of pyridine was monitored by measuring IR absorbance spectra, with a resolution of 1 cm^{-1}, using a Spectrolab 100 FTIR spectrometer. Before the measurements, pyridine was adsorbed on the surface of the samples by soaking the inorganic material in liquid pyridine for 20 min and then the samples were dried for 3 h at 80 °C in flowing air to remove any physisorbed pyridine from the oxide surface.

Photocatalytic Activity Measurements. A cylindrical Pyrex flask of ca. 20-mL capacity equipped with a quartz window was used as the photoreactor vessel. The suspension in the photoreactor was magnetically stirred. A Philips HPK high-pressure Hg lamp (125 W) illuminated the solution through a 2.2-cm-thick circulating water cell and a cutoff filter (λ > 340 nm). The light flux entering the photoreactor was 30 mW cm^{-2}. Suspensions containing 2 g L^{-1} of metal oxide spheres and 10^{-3} M 2-chlorophenol were used for the photodecomposition reactions. The aerated suspension was stirred in the dark for 90 min before illumination to reach an adsorption equilibrium of 2-chlorophenol with the metal oxide surface. The concentration of the chloride anion, a product of the decomposition of 2-chlorophenol, was measured by using an Orion chloride selective electrode. Commercial TiO_2, Degussa P25, was employed as a reference with which to compare the photocatalytic activity of the prepared samples. The pH value of the irradiated solution was maintained by the addition of H_2SO_4 or NaOH solutions employing a specially designed pH-stat.

(12) Meyer, U.; Larsson, A.; Hentze, H.-P.; Caruso, R. A. *Adv. Mater.* **2002**, *14*, 1768.
(13) Shchukin, D. G.; Caruso, R. A. *Chem. Commun.* **2003**, 1478.
(14) Fujishima, A.; Rao, T. N.; Tryk, D. A. *J. Photochem. Photobiol., C* **2000**, *1*, 1.
(15) Linsebigler, A. L.; Lu, G.; Yates, J. T., Jr. *Chem. Rev.* **1995**, *95*, 735.
(16) Fuerte, A.; Hernandez-Alonso, M. D.; Maira, A. J.; Martinez-Arias, A.; Fernandez-Garcia, M.; Conesa, J. C.; Soria, J.; Munuera, G. *J. Catal.* **2002**, *212*, 1.
(17) Yang, J.; Li, D.; Wang, X.; Yang, X. J.; Lu, L. D. *J. Solid State Chem.* **2002**, *165*, 193.
(18) Anderson, C.; Bard, A. J. *J. Phys. Chem. B* **1997**, *101*, 2611.
(19) Poznyak, S. K.; Kokorin, A. I.; Kulak, A. I. *J. Electroanal. Chem.* **1998**, *442*, 99.

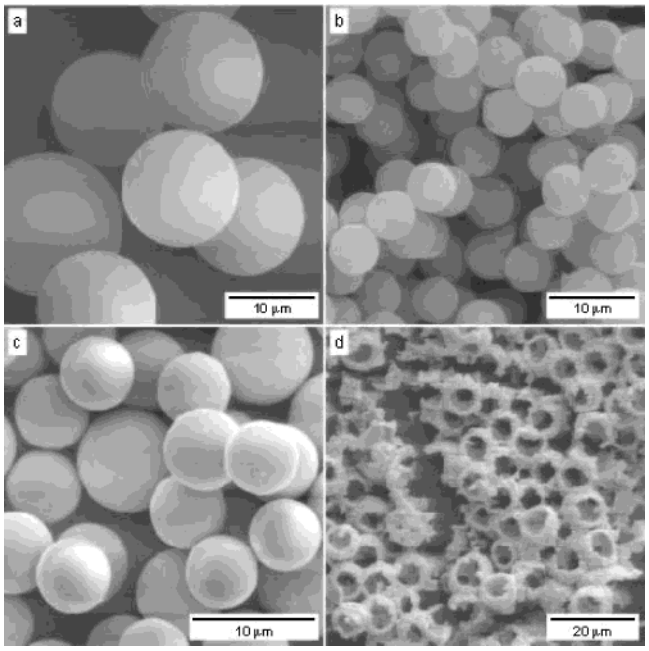

Figure 1. SEM images of (a) the initial polystyrene beads; and the template-formed inorganic materials: (b) TiO_2, (c) CeO_2, and (d) In_2O_3.

Results and Discussion

The template beads were dried, and preformed nanoparticles were synthesized (for properties of the metal oxide sols see Table 1) before infiltration of the nanoparticles into the template. The template used was a hydroxyl-functionalized, polystyrene-cross-linked-with-divinylbenzene bead with a diameter of 11.5 μm. The organic beads can be seen from scanning electron microscopy characterization to be spherical (Figure 1a), and the outer morphology was found to be porous (not shown). This porosity is essential for the templating approach, where the template is soaked in the nanoparticle solution, allowing infusion of the particles through the pores. Inspection of broken beads with the SEM revealed an inner porous structure (not shown). The specific surface area of the beads determined using nitrogen adsorption data is 50 m^2g^{-1}. [12]

The S15ETH beads were templated when the TiO_2, ZrO_2, SnO_2, and CeO_2 sols were employed. The metal oxide dispersion infiltrated the beads, resulting in sufficient nanoparticle deposition on the walls of the template so that removal of the organic scaffold by calcination gave spherical metal oxide structures. Figures 1b and c show the titania and ceria oxide spheres, respectively. Comparison of the initial polymer beads with these inorganic spheres indicates the inherent structural similarities (spherical and porous); however, the diameter of the latter is ~2.5 times lower than that of the template. Such shrinkage was observed for all the metal oxide spheres prepared, and could be due to a partial coating of the template surface with nanoparticles during impregnation. This degree of shrinkage is greater than that observed when preformed nanoparticles were used in polymer gels,[9] but within the range of that obtained for changes in film thickness when using membrane templates.[10] When DMAP-stabilized gold nanoparticles were infiltrated within the same bead template, a 25% diameter shrinkage was observed after calcining for 75 h at 280 °C.[13] Using a nonfunctionalized polystyrene/divinylbenzene bead as a template and conducting sol−gel chemistry within the template gave a decrease in diameter of 20−30% for the formation of titania spheres.[12]

Impregnation of the polystyrene template with Al_2O_3 and Fe_2O_3 sols, however, resulted in the formation of cracked inorganic spheres surrounded by excess oxide material (not shown) after template removal. In the case of the In_2O_3 sol, a hollow, shell-like structure was obtained, Figure 1d. This phenomenon is believed to be due to the agglomeration and densification of the Al_2O_3, In_2O_3, and Fe_2O_3 particles, which occurred during the calcination step. Such densification has been observed for Al_2O_3 and Fe_2O_3, as neither Al_2O_3 nor Fe_2O_3 were successful in the templating of membranes,[10] and is typical for Al_2O_3, which is used to form dense oxide layers during annealing.[20] Indium oxide has been found to successfully template when infiltrated within polymer gel or membrane templates.[9,10] The difference between these templates and the porous organic beads is the pore size of the templates. The polymer gel and membranes contain pores greater than a micrometer in diameter whereas the S15ETH bead has pore diameters on the scale of 100 nm. Hence, with densification and agglomeration of the In_2O_3 particles, loss of structuring on the nanoscale results.

Transmission electron microscopy was used to view the inner regions of the hybrid spheres after they had been ultramicrotomed. Figure 2a shows the titania/bead hybrid as an example; the inner porous structure of the template can be observed, and at higher magnification the preformed nanoparticles are seen to impregnate the inner portion of the bead (not shown). For the aluminum, indium, and iron oxide sols poor infiltration through the pores of the template and adsorption to the surfaces during the 48-h soaking time, followed by the calcination procedure which gave an increase in particle size, resulted in the loss of template structure. After removal of the template the porous structure was retained for TiO_2, ZrO_2, SnO_2, and CeO_2 with an observed decrease in pore diameter due to the overall structure shrinkage, Figure 2b. Additionally, the size of the nanoparticles forming the inorganic spheres increased up to 1.5 times that of the original nanoparticle diameter upon calcination (Figure 2c) for all of the metal oxides.

The morphological properties, including specific surface area (SA), crystal modification, and remaining weight percent (calculated from TGA of the hybrid sample), of the inorganic spheres are listed in Table 2. The samples were all crystalline with the crystal phase corresponding to the low-temperature metal oxide modification, except for the TiO_2 sample where both anatase and rutile phases were found. The crystallinity of the samples was as expected from earlier studies.[9,10] The specific surface area of the templated metal oxide spheres varied within the range of 38−81 m^2 g^{-1}, depending on the material. The spheres of the different metal oxides had similar diameters (5−6 μm). The surface area of these samples is higher than the surface area of the porous structures obtained using the same

(20) Sanchez-Lopez, J. C.; Fernandez, A. *Mater. Sci. Forum* **1998**, *269−2*, 827.

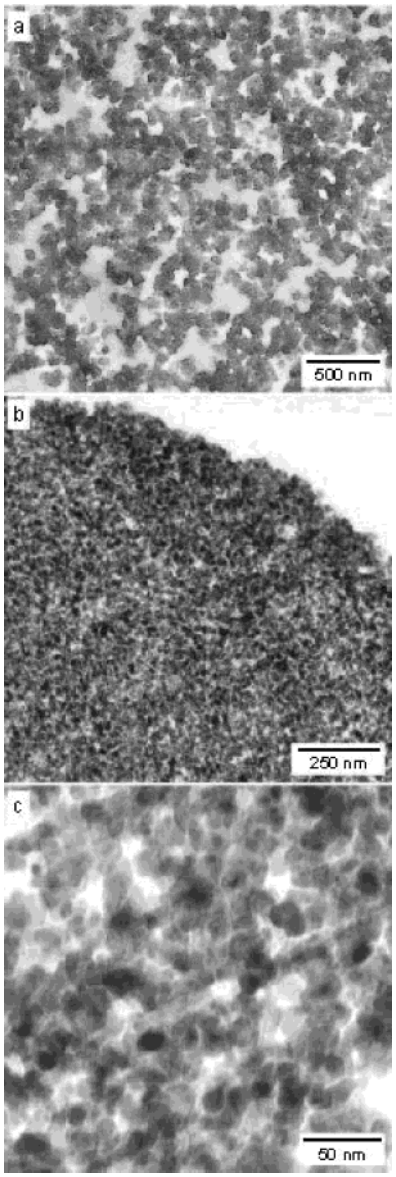

Figure 2. TEM images of the inner sphere structure of (a) the initial polymer/TiO_2 sol composite, (b) the final TiO_2, and (c) a higher magnification of the TiO_2.

Table 2. Characteristics of the Porous Metal Oxide Spheres

	tem plating[a]	surface area[b] (m^2g^{-1})	avg sphere diameter[c] (μm)	crystal modification[d]	wt. % remaining[e]
TiO_2	+	81	5	anatase, rutile	24
ZrO_2	+	49	5	monoclinic	12
Fe_2O_3	-	10	3.6	hematite	3
Al_2O_3	-	12	2.5	rhombohedral	6
In_2O_3	-	3	9[f]	cubic	18
SnO_2	+	54	6	tetragonal	14
CeO_2	+	38	6	cubic	41

[a] + = successful templating, − = not successful templating. [b] BET. [c] SEM. [d] WAXS. [e] TGA. [f] Shell diameter.

nanoparticles in membrane templates.[10] Although calcination programs were not identical in the templating of the beads and membranes, substantial differences in the template material, plus the pore structure and size, are expected to also contribute to such variation in surface area. For the metal oxide sols which did not result in spheres, Fe_2O_3, Al_2O_3, and In_2O_3, low specific surface areas were obtained and the final weight percent

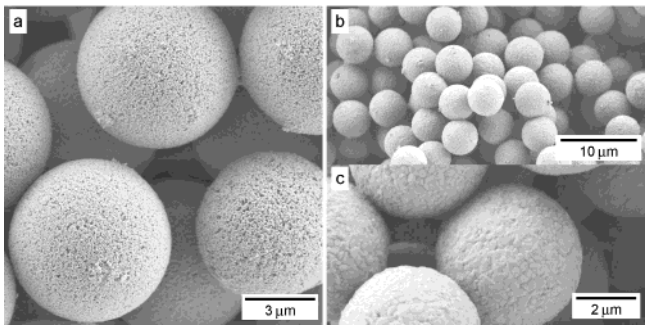

Figure 3. SEM images of template-formed mixed TiO_2/In_2O_3 inorganic spheres: (a) 1:10 (wt. %), (b) 1:1 (wt. %) low magnification, and (c) 1:1 (wt. %) higher magnification.

of inorganic remaining after heating of the hybrid samples was low, especially for Fe_2O_3 and Al_2O_3.

The addition of the titanium dioxide sol to the Fe_2O_3, Al_2O_3, or In_2O_3 sol as a second component for the impregnation stage prevents collapse of the spherical shape of the template and a porous inner structure is obtained. As shown in Figure 3, the use of a mixture of the TiO_2 and In_2O_3 sols, with a 10:1 or 1:1 TiO_2/In_2O_3 weight ratio, leads to the formation of dispersed TiO_2/In_2O_3 spheres similar to the TiO_2 spheres, with a smaller diameter (~4 μm compared with ~5 μm for TiO_2). The addition of indium oxide to the titania resulted in an overall decrease in surface area, from 81 m^2g^{-1} for TiO_2 to 78 m^2g^{-1} for a 10:1 TiO_2/In_2O_3 weight ratio, down to 53 m^2g^{-1} for 1:10 TiO_2/In_2O_3 weight ratio. Densification and crystal growth for the In_2O_3 (see also Figure 3c) is believed to be responsible for this decrease in surface area. The X-ray diffraction curves showed the anatase form of titania in the mixed TiO_2/In_2O_3 samples, indicating that the presence of the indium oxide inhibited the anatase-to-rutile phase transformation for the temperatures used during calcination. Templating the polymer beads with mixtures of the TiO_2 and Fe_2O_3 or Al_2O_3 sols gave similar results. Two possible explanations for the successful templating of the mixed metal oxide samples compared to the unsuccessful templating of the Fe_2O_3, Al_2O_3, or In_2O_3 can be considered: the TiO_2 particles form a scaffold themselves, maintaining the initial template structure; or the presence of a second component, in this case titania, inhibits the agglomeration and crystal growth of the other metal oxide particles. These two factors may contribute toward the structural stability to differing degrees with changes in the TiO_2:metal oxide ratio.

The titania and titania/indium oxide spheres were investigated for photocatalytic activity and compared with a reference photocatalyst (Degussa P25 titania) using 2-chlorophenol photodegradation as the test reaction. The emission of the chloride anion occurring during the photooxidation of 2-chlorophenol was chosen as the monitored parameter for the photocatalytic process. Figure 4 shows that the synthesized porous spheres (TiO_2; TiO_2/In_2O_3 mixture with 1:1 ratio) have higher activity toward 2-chlorophenol photodegradation than the Degussa P25 photocatalyst despite an overall larger particle size (~5-μm porous spheres compared to approximately 0.1-μm aggregates of 30-nm crystallites[21]).

(21) Hoffmann, M. R.; Martin, S. T.; Choi, W.; Bahnemann, D. W. *Chem. Rev.* **1995**, *95*, 69.

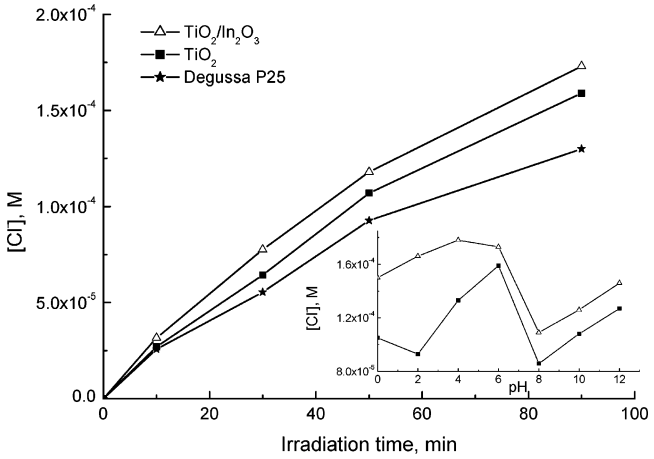

Figure 4. 2-Chlorophenol photodegradation at pH 6 in the presence of the photocatalysts Degussa P25 titania, and the template-formed spheres TiO_2 and TiO_2/In_2O_3. The insert shows the pH dependence for the photocatalysis of 2-chlorophenol using the TiO_2 and TiO_2/In_2O_3 spheres (90 min irradiation time).

This difference in the photoactivity can be explained by both the larger specific surface areas of the spheres, compared to the Degussa P25 powder, (~45 m^2g^{-1}),[4] and the high photoefficiency of the initial TiO_2 sol.[19] Adding the second metal oxide (In_2O_3) to the titania spheres further improved the photocatalytic activity, reaching 130% of the Degussa P25 activity. The presence of In_2O_3 as the second metal oxide brings about a number of changes in regard to photocatalytic activity: (i) it stabilizes the anatase phase (which generally is considered a better photocatalyst than the rutile phase)[21] modification of TiO_2 upon calcination; (ii) it changes the density and acidity of the surface hydroxyl groups of the composite, thereby enhancing the adsorption of 2-chlorophenol on the surface of the TiO_2/In_2O_3 system;[22] and (iii) it accelerates photogenerated electron/hole spatial separation by transferring the photoelectron to the In_2O_3.[22] These factors all contribute to the enhanced photocatalytic activity. From previous work[9,10] the titanium dioxide/indium oxide system was found to be more photocatalytically efficient than the synthesized TiO_2.

The dependence of the solution pH value on the 2-chlorophenol photodegradation is depicted in the insert to Figure 4. The overall degradation efficiency changes significantly with pH. The fastest oxidation rate was observed at pH 6 for the TiO_2 spheres and pH 4 for the mixed TiO_2/In_2O_3 sample. In both systems the activity drops beyond a solution pH of 6 to 7. However, with a decrease in pH value, different behavior for the titania and TiO_2/In_2O_3 samples was observed. A significant dip in photocatalytic activity is observed for the titania spheres, whereas, comparatively, the TiO_2/In_2O_3 spheres retain approximately the same activity over the same pH values. This difference can be explained by considering the different surface properties of In_2O_3 and TiO_2 (acidity, density of OH groups) which determine the rates of separate cathodic (O_2 reduction) and anodic reactions of the overall 2-chlorophenol photooxidation process.

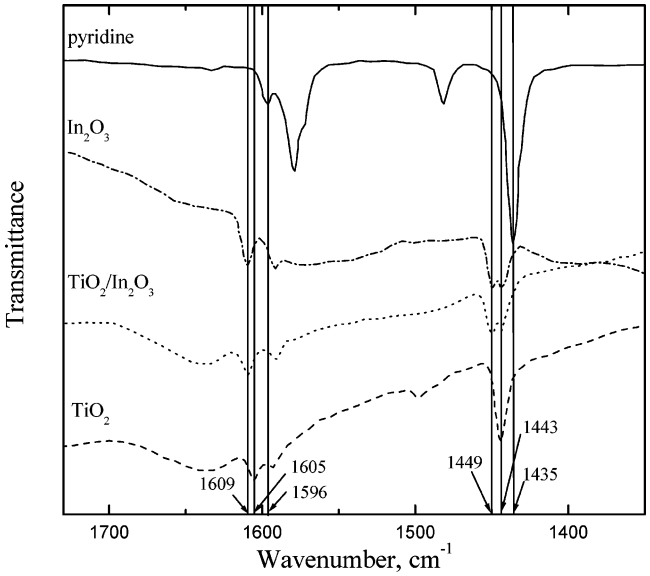

Figure 5. FTIR spectra of TiO_2, In_2O_3, and TiO_2/In_2O_3 spheres after the adsorption of pyridine. The spectrum of free pyridine is given for comparison.

The surface acidity of the TiO_2/In_2O_3 spheres was examined as a correlation between the surface acidity and photocatalytic activity of photocatalysts has been shown.[23] The adsorption of pyridine, monitored by FTIR, was chosen to characterize the surface acidity, as this has been demonstrated previously.[24] The diffuse reflection FTIR spectra of the titania and indium oxide spheres, and the TiO_2/In_2O_3 (1:1) composite after adsorption of pyridine, are shown in Figure 5. The 1400−1650 cm^{-1} wavenumber range is where pyridine ring-stretching modes are seen. The spectrum of free pyridine is also presented for comparison. The bands at 1443, 1492, and 1606 cm^{-1} observed for the TiO_2 sphere sample can be assigned to coordinated pyridine adsorbed on Lewis−acid surface sites.[25] The mode at 1443 cm^{-1} is the strongest for the TiO_2 samples. For the In_2O_3 spheres, however, there are two overlapping peaks corresponding to this mode, indicating two kinds of Lewis−acid sites present on the surface of the indium oxide. Characteristically, the shift of the bands corresponding to modes at 1605 and 1443 cm^{-1} is higher for pyridine adsorbed on In_2O_3 than that for TiO2, indicating that In_2O_3 has stronger acid sites. The FTIR spectrum of pyridine adsorbed on the TiO_2/In_2O_3 spheres is similar to that observed for the In_2O_3 samples (Figure 5).

From the reported "dark" catalytic efficiency of an In_2O_3 nanostructured electrode toward O_2 reduction,[22] it was suggested that the presence of In_2O_3 in TiO_2 accelerates the associated transfer of photogenerated electrons to oxygen. Therefore, the surface properties of the In_2O_3 may govern the O_2 photoreduction rate. Hence, at low pH values the higher surface acidity of In_2O_3 compared to that of TiO_2 is responsible for accelerating the photoreduction stage of the photocata-

(22) Shchukin, D.; Poznyak, S.; Kulak, A.; Pichat, P. *J. Photochem. Photobiol.* **2004**, *164*, 210.
(23) Papp, J.; Soled, S.; Dwight, K.; Wold, A. *Chem. Mater.* **1994**, *6*, 496.
(24) Knozinger, H. *Adv. Catal.* **1976**, *25*, 184.
(25) Morterra, C.; Coluccia, S.; Chiorina, A.; Boccuzzi, F. *J. Catal.* **1978**, *54*, 348.

lytic process, with an overall decrease in electron/hole recombination and subsequent increase in the yield of 2-chlorophenol photooxidation.

In conclusion, nanoparticle solutions of TiO_2, ZrO_2, SnO_2, and CeO_2 could successfully infiltrate porous PS/DVB beads and thus produce homogeneous porous metal oxide spheres after removal of the template. Densification of the Fe_2O_3, Al_2O_3, and In_2O_3 nanoparticles during the heating step resulted in structure loss, and hence templating was not achieved. The titania and titania/indium oxide spheres were photocatalytically active and more efficient than Degussa P25 titania for the photodecomposition of 2-chlorophenol at a solution pH of 6. Variation in the pH for the photocatalytic reaction revealed a pH value of 6 to be most effective for the photocatalytic reaction on the titania and a pH value of 4 to be most effective for the titania/indium oxide spheres.

Acknowledgment. The Max Planck Society, the Australian Research Council, the Particulate Fluid Processing Centre, and the University of Melbourne's Melbourne Research Grants Scheme are acknowledged for financial support. D.G.S. acknowledges the German Academic Exchange Service (DAAD) for a one-year research scholarship (A/01/10817) and R.A.C. acknowledges the Australian Research Council for an Australian Research Fellowship. Rona Pitschke is thanked for ultramicrotoming the samples and for TEM analysis, and Ingrid Zenke is thanked for conducting the WAXS measurements. We are grateful to Degussa Hüls for supplying the P25 titania sample.

CM0497780